JACS
JOURNAL OF THE AMERICAN CHEMICAL SOCIETY
Article
pubs.acs.org/JACS

On the Origins of Faster Oxo Exchange for Uranyl(V) versus Plutonyl(V)

Daniel Rios,[†] Maria del Carmen Michelini,*[,‡] Ana F. Lucena,[§] Joaquim Marçalo,[§] and John K. Gibson*[,†]

[†]Chemical Sciences Division, Lawrence Berkeley National Laboratory, Berkeley, California 94720, United States

[‡]Dipartimento di Chimica, Università della Calabria, 87030 Arcavacata di Rende, Italy

[§]Unidade de Ciências Químicas e Radiofarmacêuticas, Instituto Tecnológico e Nuclear, Instituto Superior Técnico, 2686-953 Sacavém, Portugal

Supporting Information

ABSTRACT: Activation of uranyl(V) oxo bonds in the gas phase is demonstrated by reaction of $U^{16}O_2^+$ with $H_2{}^{18}O$ to produce $U^{16}O^{18}O^+$ and $U^{18}O_2^+$. In contrast, neptunyl(V) and plutonyl(V) are comparatively inert toward exchange. Computed potential energy profiles (PEPs) reveal a lower yl oxo exchange transition state for uranyl(V)/water as compared with neptunyl(V)/water and plutonyl(V)/water. A correspondence between oxo exchange rates in gas phase and acid solutions is apparent; the contrasting oxo exchange rates of UO_2^+ and PuO_2^+ are considered in the context of covalent bonding in actinyls. Hydroxo exchange of $U^{16}O_2(^{16}OH)^+$ with $H_2{}^{18}O$ to give $U^{16}O_2(^{18}OH)^+$ proceeded much faster than oxo exchange, in accord with a lower computed transition state for OH exchange. The PEP for the addition of H_2O to UO_2^+ suggests that both $UO_2^+\cdot(H_2O)$ and $UO(OH)_2^+$ should be considered as potential products.

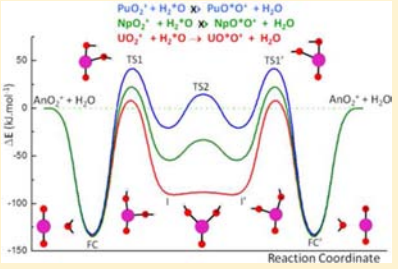

INTRODUCTION

The first study of exchange between the dipositive U(VI) species and water was performed by Crandall in 1949,[1] with the goal of distinguishing between the proposed compositions UO_2^{2+} and $U(OH)_4^{2+}$. The supposition was that ionic hydroxo ligands in the latter should exchange rapidly, whereas covalently bonded uranyl oxo ligands, which we here refer to as O_{yl}, should exchange slowly—the observed slow exchange was the first definitive evidence for UO_2^{2+} in solution. On the basis of later experimental results, Gordon and Taube[2] presented an elementary mechanism for O_{yl} exchange of UO_2^{2+} with water, catalyzed by UO_2^+, which exchanges faster than UO_2^{2+} by a factor of at least 3×10^9. Since this early work there have been experimental studies of uranyl O_{yl} exchange with the goal of understanding speciation and mechanisms under differing solution conditions, particularly at high pH, where the exchange rate is enhanced, presumably via hydrolyzed uranyl species.[3−6] Recently there has been a substantial effort to propose theoretical speciation and mechanisms for O_{yl} exchange, for AnO_2^{2+} under acidic conditions,[7,8] and for hydrolyzed uranyl species under alkaline conditions.[9−13] Although the postulated solution species and intermediates are consistent with experimental observations, direct evidence for the validity of proposed mechanisms is lacking. In the present work, we examine O_{yl} exchange under relatively uncomplicated conditions in the gas phase by experiment and density functional theory (DFT). Although studies of gas-phase reactions do not necessarily directly reveal details of complex processes that occur in solution, they do present the distinct advantage of enabling a detailed understanding of reaction mechanisms, some aspects of which may be directly pertinent to solution processes. In particular, gas-phase studies of O_{yl} exchange of monopositive and dipositive $AnO_2^{+(2+)}$ ions (An = U, Np, Pu) provide a basis for evaluating and elaborating necessarily speculative mechanisms proposed for solution exchange under acidic conditions.

Another intriguing aspect of O_{yl} exchange in solution is the variation across the actinyl series. Rabideau and Masters[14] reported the surprising result that the exchange rate for PuO_2^+ is lower than that of UO_2^+ by a factor of at least 10^7. Rabideau reported that the exchange rate for NpO_2^+ is intermediate between those for UO_2^+ and PuO_2^+.[15] As discussed below, these comparative rates have been considered enigmatic in the context of most conventional bonding evaluations of actinyl ions.[6]

In the work reported here, isotopically enriched $H_2{}^{18}O$ was reacted with $An^{16}O_2^+$ (An = U, Np, Pu) and AnO_2OH^+ (An = U, Pu) to analyze the $^{16}O/^{18}O$ exchange kinetics. Experimental studies using similar approaches with other types of oxide systems have been previously reported.[16−20] We report comparative O_{yl} exchange rates in the gas phase that are consistent with solution behavior and present DFT results that effectively explain the gas-phase experimental results. It is reasoned that the comparative O_{yl} exchange rates would be consistent with an increase in 5f orbital covalent bonding across the actinyl series, from UO_2^+ to PuO_2^+.

Received: June 14, 2012
Published: September 10, 2012

   dx.doi.org/10.1021/ja305800q | J. Am. Chem. Soc. 2012, 134, 15488−15496

EXPERIMENTAL SECTION

Caution! The ^{238}U, ^{237}Np, and ^{242}Pu isotopes used in this work are α-emitting radionuclides. Special safety precautions must be followed when handling these isotopes. The experiments reported here were performed in a special radiological containment glovebox.

The following stock acid solutions were diluted to prepare 180 μM actinyl solutions used for electrospray ionization (ESI): 177 mM $U^{VI}O_2(ClO_4)_2$ at pH = 0.6, 0.83 mM $Np^{VI}O_2(ClO_4)_2$ at pH = 1.6, and 0.70 mM $Pu^{VI}O_2(ClO_4)_2$ at pH = 1.6. The 180 μM uranyl solution had a measured pH = 3.9, reasonably close to the value of ~3.6 expected based on the ~1000× dilution of the stock solution; NaOH was added to the 180 μM neptunyl and plutonyl solutions to obtain pH ≈ 4. The actinide isotopes (>99%) were U-238 (α-decay half-life = 4×10^9 y), Np-237 (α-decay half-life = 2×10^6 y) and Pu-242 (α-decay half-life = 4×10^5 y). The ESI mass spectrometry experiments were performed using an Agilent 6340 quadrupole ion trap mass spectrometer (QIT/MS). A feature of the instrument is that ions in the trap can undergo ion−molecule reactions by applying a variable reaction delay time of up to 10 s; as no excitation is applied, observed reactions occur at the trap temperature of ~300 K.[21] The source region of the QIT/MS is inside of a radiological-containment glovebox, as described elsewhere.[22] Mass spectra were recorded in the positive ion accumulation and detection mode. Spectra were acquired using the following instrumental parameters: solution flow rate, 60 μL h^{-1}; nebulizer gas pressure, 15 psi; capillary voltage and current, −4500 V, 14.648 nA; end plate voltage offset and current, −4500 V, 37.5 nA; dry gas flow rate, 5 L min^{-1}; dry gas temperature, 325 °C; capillary exit, 141.7 V; skimmer, 26.3 V; octopole 1 and 2 dc, 13.75 and 2.13 V; octopole RF amplitude, 58.3 Vpp; lens 1 and 2, −4.8 and −65.5 V; trap drive, 216.8. High-purity nitrogen gas for nebulization and drying in the ion transfer capillary was supplied from the boil-off of a liquid nitrogen Dewar. As has been discussed elsewhere, the background water pressure in the ion trap is estimated as $\sim 10^{-6}$ Torr.[23] The helium buffer gas pressure in the trap is constant at $\sim 10^{-4}$ Torr. The ion trap has been modified to allow for the introduction of reagent gases through a leak valve. Isotopically enriched $H_2{}^{18}O$ (Aldrich, 97% ^{18}O) was introduced into the ion trap from a liquid reservoir in which the water had been subjected to repeated freeze−vacuum−thaw cycles to eliminate dissolved gases. The pressure in the trap of added $H_2{}^{18}O$ relative to that of background $H_2{}^{16}O$, which is always present in the trap at a nearly constant pressure estimated to be $\sim 10^{-6}$ Torr, was determined as discussed in the results section. To maintain a constant $H_2{}^{18}O$ pressure in the trap such that comparative exchange rates could be determined, the leak valve was maintained in a fixed partially open position and the liquid $H_2{}^{18}O$ reservoir was left open to establish a stable $H_2{}^{18}O$ pressure on the high-pressure side of the valve.

COMPUTATIONAL DETAILS

Density functional theory computations were performed using the B3LYP[24,25] functional. The Stuttgart small-core (60 core electrons) relativistic effective core pseudopotentials (RECPs) and associated valence basis sets[26] were used for the actinide atoms, while the 6-311++G(d,p) basis sets[27−29] were employed for the rest of the atoms (referred to as B3LYP/SDD hereafter). Geometry optimizations were performed without symmetry restrictions. Computations of open-shell systems were performed using spin-unrestricted methods. The nature of the calculated stationary points was characterized by a vibrational analysis performed within the harmonic approximation. For all the studied reactions the reported potential energy profiles (PEPs) were calculated as relative energies of the species involved in the reaction pathways with respect to the ground state reactant asymptotes at 0 K. The zero-point vibrational energy corrections were included in all the reported relative energies. All the minima connected by a given transition state were confirmed by performing IRC (intrinsic reaction coordinate) computations.[30,31] Further computations were performed in order to evaluate the influence of spin−orbit effects on the PEPs. In particular, single-point computations were performed on the B3LYP/SDD-optimized structures using the zero-order regular approximation (ZORA) with and without the spin−orbit correction (SO-ZORA). The scalar ZORA and SO-ZORA approximations were used together with the PBE functional and triple-ζ basis sets (TZP for actinide atoms and TZ2P for O and H). These computations will be hereafter referred to as PBE-ZORA/TZP and PBE-SO-ZORA/TZP, respectively. The choice of a pure GGA functional (PBE) in combination with the ZORA and SO-ZORA approximations was done to enable the use of the frozen core approximation, which is not recommended in combination with a part of Hartree−Fock exchange, and therefore with hybrid functionals, in the implementation of ADF code.[32,33] Consequently, in order to distinguish between the effect of the change of functional (B3LYP vs PBE) and methods (RECPs vs ZORA or SO-ZORA), single-point PBE/SDD computations were also performed on the B3LYP/SDD-optimized structures. B3LYP/SDD and PBE/SDD computations were carried out with the Gaussian 09 (revision B.01) package,[34] whereas PBE-ZORA/TZP and PBE-SO-ZORA/TZP were performed using ADF 2009.01 code.[32,33] The choice of the levels of theory was based on the good performance found in previous computational studies performed by us[35−37] and others[9,10,38,39] of similar systems.

For all the Gaussian calculations, "ultrafine" integration grids criteria were used. In some cases the multistep smearing method was used at the PBE-ZORA/TZP to achieve integer occupations numbers. The expectation values of the spin operator ($\langle S^2 \rangle$) were checked to evaluate whether spin contamination issues could affect the quality of the results (Table S3, Supporting Information). At the B3LYP/SDD level the deviation of the expectation value after the annihilation of the first spin contaminant ($\langle S^2 \rangle_A$) was lower than 1% for all the reported species. At the PBE/SDD level the spin contamination was lower than 1% for doublet, triplet, and most of quartet spin states; in only one quartet spin state case we found a spin contamination of almost 5% (first transition state, TS1). At the PBE-ZORA/TZP level the spin contamination was lower than 1% for doublet, 4% for triplet, and 10% for quartet spin states.

Despite the energetic differences observed with the change of the density functional and the inclusion of spin−orbit corrections, the energetic trend in going from UO_2^+ to PuO_2^+ is the same for all the employed levels of theory, and these differences do not affect the key conclusions drawn from the B3LYP/SDD results when comparing different PEPs. Therefore, for the sake of simplicity, in the next sections we present the PEPs of all the reactions computed at the B3LYP/SDD level together with a short comment regarding the energetic effect of the change of functional and inclusion of the spin−orbit corrections; a more complete report of the different computational results is provided as Supporting Information (Tables S1 and S2).

Bonding analysis was performed using NBO (natural bond orbital),[40] AIM (atoms in molecules)[41] and ELF (electron localization function)[42,43] approaches, using wave functions obtained at the B3LYP/SDD level of theory. AIM and ELF analyses were performed using TopMod.[44] The natural bond orbital analysis was performed using NBO version 3.1 implemented in Gaussian 09.

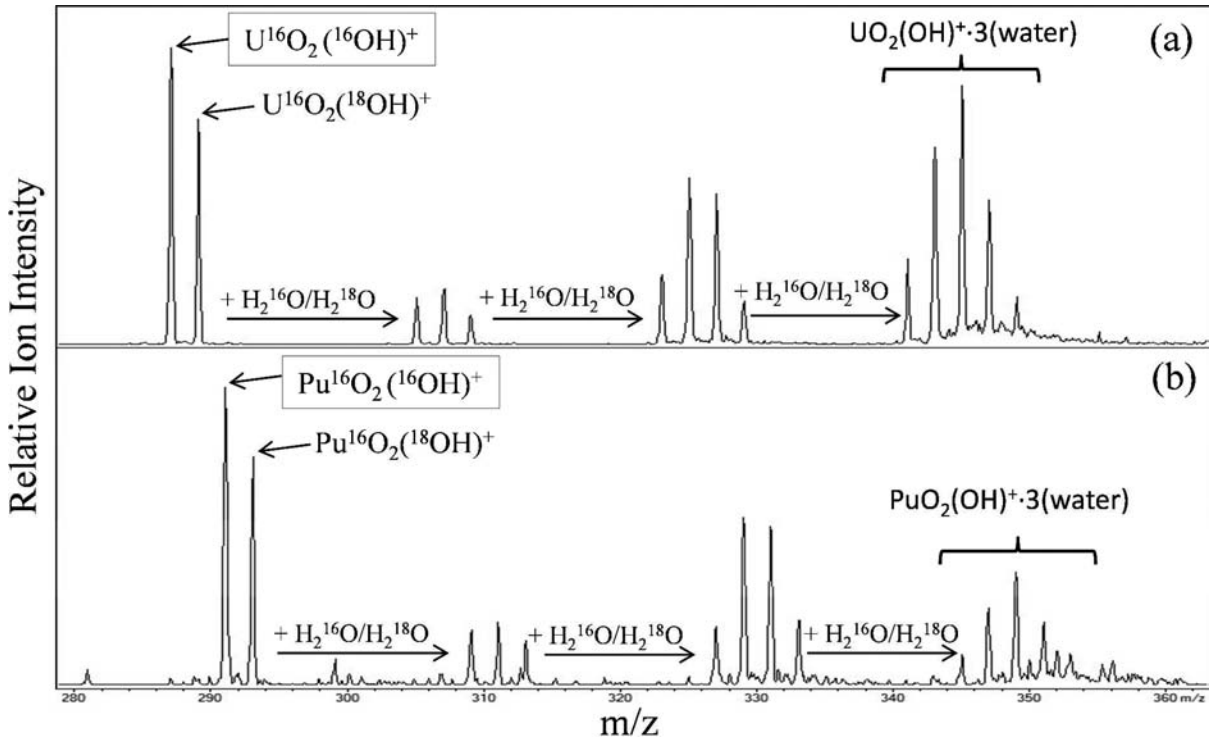

Figure 1. Mass spectra acquired after reaction for t_{appl} = 300 ms of isolated $An^{16}O_2(^{16}OH)^+$, where An = U (a) or Pu (b). The invariant relative intensities of $An^{16}O_2(^{16}OH)^+$ and $An^{16}O_2(^{18}OH)^+$ reveal that the $H_2{}^{16}O/H_2{}^{18}O$ pressure ratio in the trap is 55%/45% (eq 6b). Hydration of the $AnO_2(OH)^+$ up to $AnO_2(OH)^+{\cdot}3(H_2O)$ results in depletion of the bare hydroxides such that exchange can only be studied up to $t_{rxn} \approx 500$ ms. The $^{16}O/^{18}O$ isotopomer hydrate compositions are given in Figure S1 (Supporting Information).

RESULTS AND DISCUSSION

The relative rates of reactions of $H_2{}^{18}O$ with actinyl ions were determined experimentally using QIT/MS. Monopositive actinyl(V) and actinyl(VI) hydrate ions, $An^{16}O_2{}^+$ (An = U, Np, Pu) and $An^{16}O_2(^{16}OH)^+$ (An = U, Pu), were produced by ESI of aqueous actinyl solutions. A particular ion was isolated in the QIT by ejection of all other ions. The isolated ion and any product ions were then retained in the trap for a variable applied reaction time, t_{appl}, after which a mass spectrum was acquired to reveal the relative amounts of unreacted actinyl and product ions. The extent of reaction for different actinyls while a constant $H_2{}^{18}O$ pressure was maintained in the trap provided relative rates, expressed as limits in the present work because only lower or upper rate limits could be established for key reactions. Absolute reaction rates or rate constants were not determined due to uncertainties in the water pressure in the trap, as well as the complications in deriving kinetics when both forward and reverse reactions proceed at comparable rates. Relative reaction rates are correlated with potential energy profiles as computed by DFT. Computations were performed using the most prevalent ^{16}O isotope; a negligible isotope effect is assumed in evaluating the experiment and theory results.

Exchange of $An^{VI}O_2(OH)^+$ with Water (An = U, Pu). Representative results for reactions of $U^{16}O_2(^{16}OH)^+$ (287 *m/z*) and $Pu^{16}O_2(^{16}OH)^+$ (291 *m/z*) with $H_2{}^{18}O$ are shown in Figure 1. For t_{appl} = 300 ms, intense product peaks appear that correspond to the substitution of an ^{16}O atom by an ^{18}O atom to produce $U^{16}O_2(^{18}OH)^+$ (289 *m/z*) and $Pu^{16}O_2(^{18}OH)^+$ (293 *m/z*). The assignments of the peaks at 289 and 293 *m/z* as $An^{16}O_2(^{18}OH)^+$ from OH exchange (eq 1) rather than $An^{16}O^{18}O(^{16}OH)^+$ from O_{yl} exchange (eq 2) is based on the absence of any detectable peaks corresponding to the second O_{yl} exchange (eq 3) to give $An^{18}O_2(^{16}OH)^+$ (at 291 *m/z* for An = U and 295 *m/z* for An = Pu); reactions in italics (eqs 2 and 3) were not observed.

$$An^{16}O_2(^{16}OH)^+ + H_2{}^{18}O \rightarrow An^{16}O_2(^{18}OH)^+ + H_2{}^{16}O \quad (1)$$

$$\mathit{An^{16}O_2(^{16}OH)^+ + H_2{}^{18}O \rightarrow An^{16}O^{18}O(^{16}OH)^+ + H_2{}^{16}O} \quad (2)$$

$$\mathit{An^{16}O^{18}O(^{16}OH)^+ + H_2{}^{18}O \rightarrow An^{18}O_2(^{16}OH)^+ + H_2{}^{16}O} \quad (3)$$

Hydroxyl exchange was further confirmed by the reaction of isolated $U^{16}O_2(^{18}OH)^+$ in the presence of $H_2{}^{16}O$ and $H_2{}^{18}O$ to give only $U^{16}O_2(^{16}OH)^+$ according to eq 4 (Figure S1, Supporting Information).

$$U^{16}O_2(^{18}OH)^+ + H_2{}^{16}O \rightarrow U^{16}O_2(^{16}OH)^+ + H_2{}^{18}O \quad (4)$$

Equation 3 was not observed even with a pressure of $H_2{}^{18}O$ approximately twice that of $H_2{}^{16}O$ (Figure S1, Supporting Information); the product at 291 *m/z* is confirmed as $U^{16}O_2(^{18}OH)^+$ rather than $U^{16}O^{18}O(^{16}OH)^+$.

Also apparent in Figure 1 are peak manifolds corresponding to the addition of one, two, or three $H_2{}^{16}O$ and/or $H_2{}^{18}O$ molecules to $An^{16}O_2(^{16}OH)^+$ and $An^{16}O_2(^{18}OH)^+$, consistent with previous results.[37] The broad high-mass peak tails in the uranyl hydroxide trihydrate peak manifold (Figure 1a) are characteristic of terminal inner-sphere hydrates, which are susceptible to dissociation during ejection from the ion trap.[23] The several unidentified minor peaks in the plutonyl hydroxide mass spectrum (Figure 1b) reflect the very low abundance of the $Pu^{16}O_2(^{16}OH)^+$ reactant.[37] The hydrate isotopomer

dx.doi.org/10.1021/ja305800q | J. Am. Chem. Soc. 2012, 134, 15488−15496

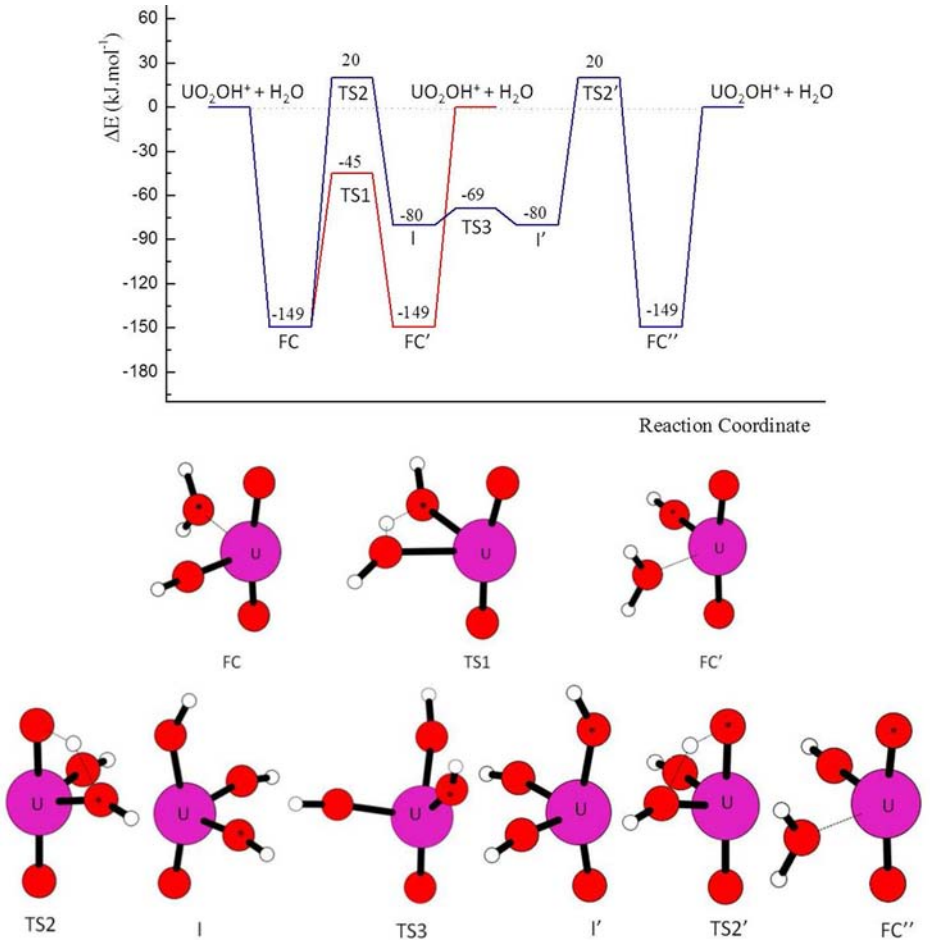

Figure 2. Potential energy profiles for the O_{yl} exchange (blue) and OH exchange (red) reactions of UO_2OH^+ and H_2O. Although the computations did not consider the potential for an isotopic effect, a black asterisk is used to identify ^{18}O in the structures of the first complex (FC, FC′, and FC″), transition states (TS1, TS2, and TS3), and intermediate (I and I′) to facilitate comparison with the experimental results.

compositions are given in Figure S1 (Supporting Information). It would be desirable to isolate hydrates and study their exchange, but these experiments are impractical due to the low intensities of the isotopically pure hydrate isotopomers, the fast hydroxo exchange and hydration rates, and the inability to distinguish between hydroxo exchange and water exchange.

A comparison of the extent of hydration of isolated $U^{16}O_2(^{16}OH)^+$ with no applied reaction time, t_0 (~20% hydration), to that with an applied t_{appl} = 50 ms (~35% hydration) indicates an inherent reaction delay of $t_0 \approx 70$ ms before a mass spectrum is acquired (Figure S2, Supporting Information). Accordingly the actual reaction time is $t_{rxn} \approx t_{appl}$ + 70 ms. The near invariance of the $U^{16}O_2(^{18}OH)^+/U^{16}O_2(^{16}OH)^+$ ion intensity ratio upon the application of any reaction time (e.g., for t_{appl} = 50 ms in Figure S2, Supporting Information) indicates that the exchange process has nearly attained equilibrium within ~70 ms such that the forward and reverse rates for eq 5 have become nearly the same.

$$U^{16}O_2(^{16}OH)^+ + H_2{}^{18}O \leftrightarrow U^{16}O_2(^{18}OH)^+ + H_2{}^{16}O \quad (5)$$

If a minimal isotope effect is assumed, then the forward and reverse rate constants for eq 5 are the same and the equilibrium constant is near unity (eq 6a). The relative pressures of $H_2{}^{16}O$ and $H_2{}^{18}O$ are then given by the $U^{16}O_2(^{16}OH)^+/U^{16}O_2(^{18}OH)^+$ intensity ratio (eq 6b).

$$K_{eq}(eq5) = k_{forward}/k_{reverse} = [H_2{}^{16}O][U^{16}O_2(^{18}OH)^+]/[H_2{}^{18}O][U^{16}O_2(^{16}OH)^+] \approx 1 \quad (6a)$$

$$[H_2{}^{16}O]/[H_2{}^{18}O] \approx [U^{16}O_2(^{16}OH)^+]/[U^{16}O_2(^{18}OH)^+] \quad (6b)$$

The result that equilibrium for eq 5 is essentially achieved within <100 ms can be evaluated in the context of the pseudo-first-order collisional rate for the reaction of $U^{16}O_2(^{16}OH)^+$ with $H_2{}^{18}O$. The collisional rate constant is $k_{COL} = 2.1 \times 10^{-9}$ cm^3 molecule^{-1} s^{-1};[45] if $P\{H_2{}^{18}O\} \approx 1 \times 10^{-6}$ Torr, then the collisional rate is ~70 s^{-1}, which corresponds to about seven collisions, on average, of each $UO_2(OH)^+$ with a $H_2{}^{18}O$ molecule in 100 ms. The observation of near-equilibrium within <100 ms thus suggests a high reaction probability.

No O_{yl} exchange was observed for $U^{16}O_2(^{16}OH)^+$ to a detection limit of 3% for t_{appl} = 400 ms ($t_{rxn} \approx$ 470 ms), which extrapolates to <1% O_{yl} exchange for t_{rxn} = 100 ms. As ^{16}OH exchange is nearly 100% complete within 100 ms, the results indicate that for the reaction of $U^{16}O_2(^{16}OH)^+$ with water, O_{yl} exchange is <1% as efficient as OH exchange; the result shown for $Pu^{16}O_2(^{16}OH)^+$ in Figure 1b indicates essentially the same behavior.

The computed potential energy profiles (PEPs) for the OH exchange and O_{yl} exchange reactions of $UO_2(OH)^+$ with H_2O are shown in Figure 2, where asterisked O-atoms correspond to

dx.doi.org/10.1021/ja305800q | J. Am. Chem. Soc. 2012, 134, 15488−15496

^{18}O in the experiments. Addition of H_2O to $UO_2(OH)^+$ is exothermic by 149 kJ mol^{-1}. Under the experimental conditions the temperature is ~300 K[21] and only reactions that proceed on a PEP that lies below the energy of the reactants—i.e., below the reactant asymptote—should be observed. The transition state for OH exchange, TS1, is 45 kJ mol^{-1} below the reactant asymptote such that the reaction should occur efficiently, in accord with experimental observations.

In contrast to OH exchange, the first transition state for O_{yl} exchange, TS2 in Figure 2, is 20 kJ mol^{-1} above the reactant asymptote. Whereas TS1 for OH exchange disrupts the U−OH bond, TS2 for O_{yl} exchange disrupts a much stronger U≡O bond. The observation of facile OH exchange versus the nonobservation of O_{yl} exchange can basically be traced to this difference in the PEPs. The high energy of intermediate I, $UO(OH)_3^+$, relative to that of the first complex FC (and FC′), $UO_2(OH)^+\cdot(H_2O)$, can similarly be attributed to disruption of the robust uranyl moiety. Slow O_{yl} exchange as compared with OH exchange is precisely the premise by which Crandall assigned the dipositive U(VI) solution species as UO_2^{2+} rather than $UO(OH)_4^{2+}$.[1]

PBE/SDD results indicate that the substitution of the hybrid functional by the PBE functional (single-point computations) systematically stabilizes the species involved in the PEPs with respect to the reactant asymptotes by up to 28 kJ mol^{-1} (Table S1, Supporting Information).

As the electron configuration of U in UO_2OH^+ is $5f^0$, it is unsurprising that the relative energies of the species involved in the $UO_2OH^+ + H_2O$ PEP remain essentially unchanged by the inclusion of the spin−orbit correction. The differences between relative energies at PBE-ZORA/TZP and PBE-SO-ZORA/TZP levels are less than 4 kJ mol^{-1}.

Exchange of $An^VO_2^+$ with Water (An = U, Np, Pu). The three actinyl ions $U^{16}O_2^+$, $Np^{16}O_2^+$, and $Pu^{16}O_2^+$ were exposed to a $H_2{}^{16}O/H_2{}^{18}O$ mixture for up to the maximum t_{appl} = 10 s. The O_{yl} exchange reaction given by eq 7 was observed for UO_2^+ but not for NpO_2^+ or PuO_2^+ (Figure S3, Supporting Information).

$$An^{16}O_2^+ + H_2{}^{18}O \rightarrow An^{16}O^{18}O^+ + H_2{}^{16}O \quad (7)$$

The second O_{yl} exchange (eq 8) was also observed for uranyl. Isolation of $U^{16}O^{18}O^+$ in the presence of $H_2{}^{16}O$ and $H_2{}^{18}O$ confirmed that the exchange reactions given by eqs 8 and 9 proceed simultaneously (Figure S4, Supporting Information).

$$U^{16}O^{18}O^+ + H_2{}^{18}O \rightarrow U^{18}O_2^+ + H_2{}^{16}O \quad (8)$$

$$U^{16}O^{18}O^+ + H_2{}^{16}O \rightarrow U^{16}O_2^+ + H_2{}^{18}O \quad (9)$$

From the observed exchange rate for $U^{16}O_2^+$ and limits for $Np^{16}O_2^+$ and $Pu^{16}O_2^+$, it was established that the efficiency of O_{yl} exchange for both NpO_2^+ and PuO_2^+ is <5% as compared with that for UO_2^+ (Figure S5, Supporting Information).

The PEPs for O_{yl} exchange of UO_2^+, NpO_2^+, and PuO_2^+ are shown in Figure 3, where asterisked O-atoms correspond to ^{18}O in the experiments. Addition of H_2O to the AnO_2^+ (FC) is exothermic by ca. 140 kJ mol^{-1} in all cases. The first transition states (TS1) are above the asymptote, by 13 kJ mol^{-1} for UO_2^+, 27 kJ mol^{-1} for NpO_2^+ and by 46 kJ mol^{-1} for PuO_2^+.

The trend of the computed first transition state, TS1, from UO_2^+ to PuO_2^+ is consistent with the experimental observations. Although the 13 kJ mol^{-1} computed for UO_2^+

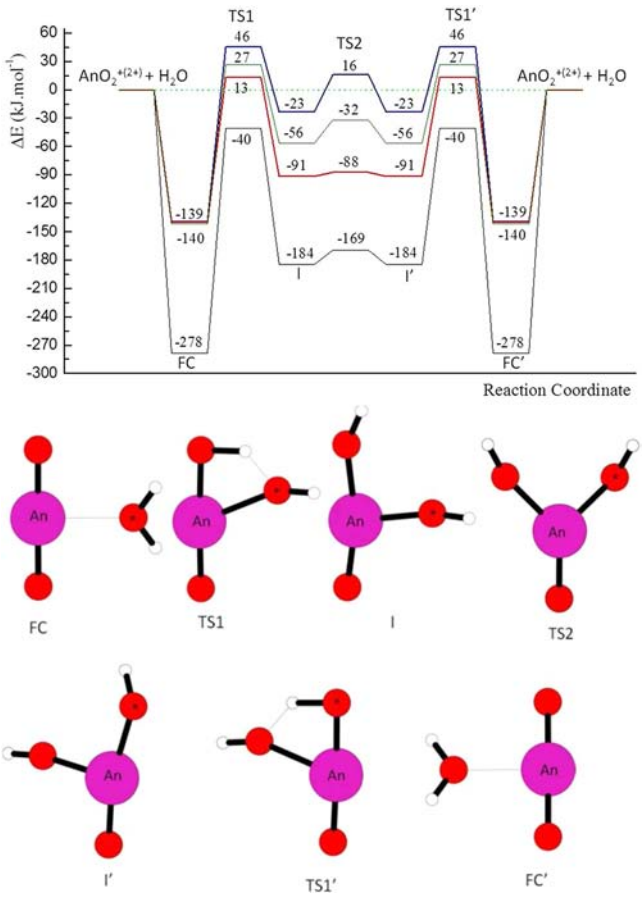

Figure 3. Potential energy profiles for the O_{yl} exchange reactions of UO_2^+ (red), NpO_2^+ (green), PuO_2^+ (blue), and UO_2^{2+} (gray) with H_2O. O-atoms labeled with asterisks correspond to ^{18}O in the experiments.

TS1 is slightly above the reactant energy asymptote, in view of the estimated uncertainties this value is consistent with the inefficient O_{yl} exchange observed for UO_2^+. Significantly higher TS1 barrier heights for NpO_2^+ and PuO_2^+ are consistent with the nonobservation of O_{yl} exchange to within the experimental detection limit. The minor barrier presented by TS2 in Figure 3 corresponds to rearrangement of the fluxional hydroxides in intermediate I prior to reversal of the reaction through I′, TS1′, and FC′, ultimately resulting in elimination of a water molecule which incorporates an O_{yl} from the reactant AnO_2^+. The gas-phase mechanism identified here is in close correspondence to the mechanism proposed by Réal et al. for photoinduced O_{yl} exchange of UO_2^{2+} in solution.[8]

Our PBE/SDD computations indicate that the substitution of the B3LYP functional by the PBE stabilizes the AnO_2^+ PEPs by up to 10 (UO_2^+), 22 (NpO_2^+), and 24 kJ mol^{-1} (PuO_2^+) (Table S2, Supporting Information). A comparison of the PBE-ZORA/TZP and PBE-SO-ZORA/TZP shows that in the case of $UO_2^+(5f^1)$ + H_2O the relative energies of the species involved in the PEP are stabilized by up to 8 kJ mol^{-1} by the inclusion of the spin−orbit correction. As expected, the highest impact of the inclusion of the spin−orbit effects is observed in the $PuO_2^+(5f^3)$ + H_2O PEP, where the inclusion of the spin−orbit correction destabilizes the PEP by between 20 and 29 kJ mol^{-1}. For $NpO_2^+(5f^2)$ the inclusion of the spin−orbit correction stabilizes/destabilizes the relative energies of the

dx.doi.org/10.1021/ja305800q | J. Am. Chem. Soc. 2012, 134, 15488−15496

species involved in the pathway by between −3 and +11 kJ mol^{-1} (Table S2, Supporting Information).

Figure 3 reveals that the disparity among UO_2^+, NpO_2^+, and PuO_2^+ essentially reflects the higher energy of TS1 and intermediate I, $AnO(OH)_2^+$, relative to the first complex, $AnO_2\cdot(H_2O)^+$, in going from U to Pu. This trend is observed at all the computational levels used here (see Table S3, Supporting Information). This result, supported by the experimental observations, suggests that it is more difficult to disrupt an O_{yl} bond in PuO_2^+ than in UO_2^+, which is somewhat counterintuitive given that the oxo bonds in uranyl(V) are quite stronger than in plutonyl(V).[6,46] As discussed below, these O_{yl} exchange results are consistent with more covalent bonding in plutonyl than uranyl.

It was found that near-equilibrium between $U^{16}O_2(^{16}OH)^+$ and $U^{16}O_2(^{18}OH)^+$, which corresponds to ∼100% OH exchange, is established within <100 ms. Under the same conditions, eq 7 proceeds by 4.4% after 1 s, which extrapolates to 0.44% after 100 ms. These results indicate that O_{yl} exchange for UO_2^+ (eq 7) occurs at <0.5% efficiency relative to OH exchange for $UO_2(OH)^+$ (eq 1). This is in accord with TS1 lying well below the reactant asymptote for OH exchange (Figure 2) but close to the reactant asymptote for O_{yl} exchange for UO_2^+ (Figure 3). The fluxional nature of the hydroxyl ligand is as predicted by Crandall.[1]

Exchange of UO_2^{2+} with Water; Linking Gas and Solution Exchange. Although dipositive coordination complexes of UO_2^{2+}, NpO_2^{2+}, and PuO_2^{2+} have been produced by ESI using the techniques employed in the present work,[22] it was not possible to obtain bare dipositive actinyls, AnO_2^{2+}, to study exchange reactions. The PEP for the oxo exchange reaction of UO_2^{2+} with H_2O (eq 10) was computed, the results being in Figure 3. The energy for the alternative electron transfer reaction given by eq 11 is −192 ± 40 kJ mol^{-1},[47] which was computed here as −261 and −250 kJ mol^{-1} at B3LYP/SDD and SO-PBE-ZORA/TZP levels, respectively, and may occur in competition with eq 10. As electron transfer is not directly relevant to oxo exchange, the PEP for eq 11 was not computed in this work.

$$U^{16}O_2^{2+} + H_2{}^{18}O \rightarrow U^{16}O^{18}O^{2+} + H_2{}^{16}O \quad (10)$$

$$U^{16}O_2^{2+} + H_2{}^{18}O \rightarrow U^{16}O_2^{+} + H_2{}^{18}O^{+} \quad (11)$$

As TS1 for eq 10 lies 40 kJ mol^{-1} below the reactant asymptote, the DFT results predict that O_{yl} exchange for UO_2^{2+} should proceed more efficiently than for UO_2^+, for which TS1 lies close to the reactant asymptote. Similar conclusions are drawn from the different single-point computations (Table S2, Supporting Information). The PEP shifts by up to 51 kJ mol^{-1} toward more negative energies at the PBE/SDD level. A comparison of the PBE-ZORA/TZP and PBE-SO-ZORA/TZP computations indicate that the spin−orbit correction modifies the relative energies by less than 5 kJ mol^{-1} (Table S2, Supporting Information).

The prediction that gas-phase O_{yl} exchange should be more efficient for UO_2^{2+} than UO_2^+ is seemingly in discord with the opposite relative rates in acidic solution, where UO_2^+ exchanges much faster than does UO_2^{2+}.[2] Consideration of the PEPs and the different conditions for gas and solution exchange actually suggest accordance. The initial step in gas-phase oxo exchange is ion/molecule association to form the hydrate, $UO_2\cdot(H_2O)^+$ or $UO_2\cdot(H_2O)^{2+}$, referred to as FC in the PEPs. The computed first hydration energy is −139 kJ mol^{-1} for UO_2^+ and −278 kJ mol^{-1} for UO_2^{2+}; the much greater hydration energy for dipositive uranyl results in TS1 lying 40 kJ mol^{-1} below the asymptote and the prediction of facile gas-phase O_{yl} exchange for UO_2^{2+}. In solution, uranyl ions are fully hydrated such that the hydration energy furnished in the gas phase is not imparted to enable surmounting the activation barrier presented by TS1. In essence, the solution reactant asymptote is at the energy of the solvated uranyl ion. Although there are five inner-sphere coordinating water molecules in aqueous solution, in a simplified model only the coordinating water that exchanges needs to be considered, such that the reactant asymptote corresponds to the energy of the FC in the PEPs. The barrier to exchange is then the energy difference between FC and TS1, which is 152 kJ mol^{-1} for UO_2^+ and 238 kJ mol^{-1} for UO_2^{2+}; faster solution exchange under acidic conditions is predicted for UO_2^+ as compared with UO_2^{2+}, in accord with observations. This assessment does not imply that O_{yl} exchange in a complex solution environment is accurately represented by the PEPs in Figure 3 but rather that the seemingly discordant gas and solution relative exchange rates are actually in rather good accord and that essential features of mechanisms for exchange in solution may also appear in simple systems in the gas phase. The similarities between the present gas-phase mechanisms and the solution mechanism put forth by Réal et al. indicates a close correspondence.[8] It should be emphasized that much faster solution O_{yl} exchange which occurs under basic conditions presumably involves hydrolyzed species such as have been proposed by Clark and co-workers[3] and Schreckenbach and co-workers.[9−11]

It is known that exchange for PuO_2^+ in solution is slower than for UO_2^+, a result that might be considered "enigmatic" in view of the greater energy necessary to remove an oxo ligand from UO_2^+ as compared with PuO_2^+, as in eqs 12 and 13.[46]

$$UO_2^+ \rightarrow UO^+ + O \quad \Delta E = 741 \pm 14 \text{ kJ mol}^{-1} \quad (12)$$

$$PuO_2^+ \rightarrow PuO^+ + O \quad \Delta E = 509 \pm 38 \text{ kJ mol}^{-1} \quad (13)$$

We have here demonstrated that less efficient exchange for PuO_2^+ versus UO_2^+ also appears in the gas phase. An explanation for these unexpected results in both gas and solution might be related to the nature of the bonding in $\{O-An-O\}^+$ species, and the premise that stronger bonding does not necessarily indicate greater covalency.[48] A covalent contribution to bonding involving 5f-orbitals in actinyls has been a long-standing topic of discussion, with significant covalency in uranyl having been well-established.[49−54] More than 60 years ago Crandall,[1] and later Glueckauf and McKay,[55] attributed the "nonexchange with oxygen-18 in heavy water" to "covalent binding of the oxygens in the uranyl ion". It has since been suggested that 5f covalency might increase across the actinide series such that the bonding in plutonyl could be more covalent than that in uranyl,[56−61] a result of which could be less efficient O_{yl} exchange for plutonyl as observed, in accord with the premise employed by Crandall.[1] However, recent theoretical studies have shown that there is not a straightforward evaluation of covalency trends across the actinide series.[62] In particular, the unusual bonding situation observed in actinide-containing molecules is the presence of valence molecular orbitals that have significant contribution from both actinide and ligand, yet without significant atomic orbital overlap. The origin of the increase in the orbital mixing in going across in the actinide series is the matching between atomic orbital energies of the atoms forming the bond and not an

dx.doi.org/10.1021/ja305800q | J. Am. Chem. Soc. 2012, 134, 15488−15496

increased atomic overlap. Therefore, traditional quantum mechanical tools for assessing covalency usually predict significant metal−ligand covalency. However, the observed valence orbital mixing does not necessarily lead to internuclear charge buildup. This peculiar situation yields to contrasting conclusions regarding the trend in covalency along the actinide series depending on the theoretical approach employed to perform the bond analysis.[62]

We have analyzed the bonding of AnO_2^+, AnO_2OH^+ (An = U, Pu), and UO_2^{2+} ions using traditional quantum-mechanical tools (NBO) and topological methodologies (AIM, ELF). The obtained results are included as Supporting Information (Tables S4−S6) together with a brief introduction to the AIM and ELF methodologies and a discussion of the results. NBO analysis shows an increase in the bonding participation of the 5f orbitals in going from U to Pu in the AnO_2^+ species, as measured by the contribution of the metal orbitals to the natural bond orbitals and by the actinide natural populations. As underlined in previous theoretical studies,[62] however, the higher metal contribution to the bonding orbitals is the result of a higher mixing of the atomic orbitals due to the better energy matching and does not necessarily imply greater covalency in the traditional sense (i.e., greater overlap between atomic orbitals). AIM analysis indicates that there is a small increase in the An−O_{yl} bond critical point charge density, ρ_{BCP}, in going from UO_2^+ to PuO_2^+ as well as in going from $UO(OH)_2^+$ to $PuO(OH)_2^+$. ELF analysis indicates the presence of a An−O_{yl} disynaptic valence basin in all the species analyzed. The contribution of the actinide atom to those basins is in all cases very low (less than 10% of the total population), which is an indication of the high ionicity of the bond. Even when the percentage of contribution from the actinide is slightly higher in both PuO_2^+ and $PuO(OH)_2^+$, the difference is really too small to draw definitive conclusions (see the Supporting Information for details).

The comparative gas-phase O_{yl} exchange rates, $UO_2^+ \gg PuO_2^+$, is in accord with the higher-energy TS1 and intermediate I for plutonyl (Figure 3). It might be expected that similar bis-hydroxo intermediates, $PuO(OH)_2^+$(aq) and $UO(OH)_2^+$(aq), should appear in solution phase.[8] A key finding from the present results is that $PuO(OH)_2^+$ is less stable relative to $PuO_2^+\cdot(H_2O)$ than $UO(OH)_2^+$ is relative to $UO_2^+\cdot(H_2O)$; the computed energies for eqs 14 and 15 are as indicated (B3LYP/SDD).

$$UO_2^+\cdot(H_2O) \rightarrow UO(OH)_2^+ \quad \Delta E = 48 \text{ kJ mol}^{-1} \tag{14}$$

$$PuO_2^+\cdot(H_2O) \rightarrow PuO(OH)_2^+ \quad \Delta E = 117 \text{ kJ mol}^{-1} \tag{15}$$

Formation of the $AnO(OH)_2^+$ intermediates disrupts the bonding in the $\{O-An-O\}^+$ ions. Although the bonding in UO_2^+ is inherently stronger than that in PuO_2^+ (eqs 12 and 13), it is feasible that there is a greater 5f covalent contribution in the latter. A result of greater covalency would be greater difficulty disrupting the linear $\{O-Pu-O\}^+$ moiety as compared with $\{O-U-O\}^+$, which is precisely the effect indicated by the PEPs (Figure 3) and eqs 14 and 15. The observations of slower O_{yl} exchange for PuO_2^+ versus UO_2^+ in both acid solution and gas are consistent with—but do not definitively demonstrate—greater 5f covalent bonding in PuO_2^+ than in UO_2^+, in accord with the increasing covalency across the series of solid actinide dioxides proposed by Prodan et al.[60] As remarked above, bonding analysis does not definitively demonstrate a difference in covalency between UO_2^+ and PuO_2^+; the proposed difference is inferred solely from the experimental observations.

Differentiating between Isomers $UO_2(H_2O)^+$and $UO(OH)_2^+$. In previous work it has been assumed that addition of H_2O to UO_2^+ results in the hydrate, $UO_2^+\cdot(H_2O)$.[37,63] However, the PEP for the reaction of H_2O with UO_2^+ (Figure 3) indicates that the bis-hydroxide, $UO(OH)_2^+$, intermediate I in the observed exchange reaction of UO_2^+, is also an exothermic product of water addition to uranyl(V). A common assumption is that the lower-energy hydrate is the product of water addition, but it is feasible that the reaction proceeds along the PEP to the bis-hydroxide, with collisional cooling quenching the reaction there. A stronger Lewis base such as acetone will displace water ligands in the gas phase, providing a means to distinguish between hydrates and hydroxides, such as in eqs 16 and 17.

$$UO_2^+\cdot(H_2O) + n(\text{acetone}) \rightarrow UO_2^+\cdot n(\text{acetone}) + H_2O \tag{16}$$

$$UO(OH)_2^+ + n(\text{acetone}) \rightarrow UO(OH)_2^+\cdot n(\text{acetone}) \tag{17}$$

The reaction between H_2O and UO_2^+ is too slow to isolate the gas-phase addition product and study eqs 16 and 17.[37] Instead, $UO_2^+\cdot(H_2O)$ was directly produced by ESI and transferred into the ion trap as described previously.[37] After a 1 s reaction time with acetone ($P \sim 10^{-6}$ Torr) the dominant products were $UO_2(O_2)^+\cdot 3$(acetone) [100% relative abundance], $UO_2^+\cdot 3$(acetone) [80%], and $UO_2^+\cdot 4$(acetone) [20%]. The superoxo complex, $UO_2(O_2)^+\cdot 3$(acetone), in which U(V) has been oxidized to U(VI) by the addition of O_2, has been reported previously.[64,65] The abundance of the two complexes that retained a water molecule sum to less than 5% of the total product abundance. Formulated as hydrates, these minor products were $UO_2(O_2)^+\cdot 2(\text{acetone})\cdot(H_2O)$ and $UO_2^+\cdot 2(\text{acetone})\cdot(H_2O)$; they could alternatively be formulated as $UO(OH)_2(O_2)^+\cdot 2$(acetone) and $UO(OH)_2^+\cdot 2$(acetone). The results indicate that $UO_2^+\cdot(H_2O)$ produced by ESI under our experimental conditions is predominantly, if not entirely, the indicated hydrate, comprising at most 5% of the $UO(OH)_2^+$ isomer. However, the contribution of the latter isomer as a result of gas-phase association of H_2O and UO_2^+ could be substantially greater and should generally be considered.

CONCLUSIONS

Experimental results have shown that for $UO_2(OH)^+$ and $PuO_2(OH)^+$ with water, OH exchange occurs much more efficiently than O_{yl} exchange, the latter not having been observed. The PEP computed for $UO_2(OH)^+$ by DFT is in accord with these results: the energy of the transition state is below the reactant asymptote for OH exchange, but not for O_{yl} exchange. Facile OH exchange as compared with O_{yl} exchange is in accord with the rationale presented by Crandall that a covalent U−O_{yl} bond should be more resistant to disruption than an ionic U−OH bond.[1]

The O_{yl} exchange efficiency for UO_2^+ was much greater than for NpO_2^+ and PuO_2^+. DFT results for UO_2^+, NpO_2^+, and PuO_2^+ indicate a substantially higher energy transition state for the latter two, in accord with the observations. The comparative O_{yl} exchange results are consistent with—but do not definitively confirm—greater 5f-orbital covalency in PuO_2^+ versus UO_2^+, which could be attributed to a better energy

dx.doi.org/10.1021/ja305800q | J. Am. Chem. Soc. 2012, 134, 15488−15496

match between the actinide 5f and oxygen 2p orbitals upon proceeding across the actinyl series.[60,62] The relative O_{yl} rates for UO_2^+ and PuO_2^+ in acid solution are qualitatively the same as in gas. We propose that the same essential features play a role in gas and solution exchange.

The PEP was computed for O_{yl} exchange of UO_2^{2+}. The transition state is well below the reactant asymptote such that gas-phase O_{yl} exchange is predicted to proceed more efficiently for UO_2^{2+} than UO_2^+, which is just the opposite of the relative O_{yl} exchange rates in solution, $UO_2^+ \gg UO_2^{2+}$. Considerations of the nature of gas-phase ion/molecule exchange, which is initiated by exothermic ion hydration, indicate that the gas-phase prediction is in accord with known solution behavior. In particular, the reactant asymptote in solution corresponds to the hydrated ion such that the uranyl ion−water interaction energy is not supplied to enable surmounting the transition state. The similarities between the present gas-phase DFT results for UO_2^{2+} and a proposed mechanism for photoinduced exchange of UO_2^{2+} in solution[8] support the premise that gas-phase reaction mechanisms can effectively model some solution processes.

In view of the DFT result that the gas-phase reaction of UO_2^+ with H_2O to produce $UO(OH)_2^+$ is exothermic, a contribution of this bis-hydroxo isomer, in addition to the conventionally presumed hydrate, $UO_2^+\cdot(H_2O)$, should be considered. It was possible to establish that $UO_2^+\cdot(H_2O)$ produced by ESI is at least 95% the hydrate isomer. It was not possible to establish if there is a significant contribution of $UO(OH)_2^+$ from the gas-phase addition of H_2O to UO_2^+.

■ ASSOCIATED CONTENT

Supporting Information

Relative energies of the species involved in all the studied reaction pathways at the B3LYP/SDD, PBE/SDD, PBE-ZORA/TZP, and PBE-SO-ZORA/TZP levels; results and discussion of the NPA, AIM, and ELF analyses; mass spectrum for reaction of $U^{16}O_2(^{18}OH)^+$ with $H_2{}^{16}O$ and $H_2{}^{18}O$; mass spectra for reaction of $U^{16}O_2(^{16}OH)^+$ with $H_2{}^{16}O$ and $H_2{}^{18}O$ for applied times of 0 and 50 ms; mass spectra for reactions of $U^{16}O_2^+$, $Np^{16}O_2^+$, and $Pu^{16}O_2^+$ with $H_2{}^{18}O$; mass spectrum for reaction $U^{16}O^{18}O^+$ with $H_2{}^{16}O$ and $H_2{}^{18}O$. Mass spectra for reactions of $U^{16}O_2^+$ and $Pu^{16}O_2^+$ with $H_2{}^{18}O$ for 1 and 10 s, respectively; B3LYP/SDD-optimized geometric parameters of all the species involved in the O_{yl} exchange pathways of AnO_2^+(An = U, Np, Pu), $UO(OH)_2^+$, and UO_2^{2+}. Full citation for ref 34. This material is available free of charge via the Internet at http://pubs.acs.org.

■ AUTHOR INFORMATION

Corresponding Author

mc.michelini@unical.it; jkgibson@lbl.gov

Notes

The authors declare no competing financial interest.

■ ACKNOWLEDGMENTS

This research was supported by the U.S. Department of Energy, Office of Basic Energy Sciences, Heavy Element Chemistry at LBNL, under Contract No. DE-AC02-05CH11231 (D.R., J.K.G.); by the Università della Calabria (M.d.C.M); and by the Fundação para a Ciência e a Tecnologia (PhD grant SFRH/BD/70475/2010 to A.F.L.) (A.F.L., J.M.). M.d.C.M. is grateful for the opportunity to be a Guest Scientist in the LBNL Chemical Sciences Division. This research used resources of the National Energy Research Scientific Computing Center (NERSC), which is supported by the Office of Science of the U.S. Department of Energy under Contract No. DE-AC02-05CH11231.

■ REFERENCES

(1) Crandall, H. W. *J. Chem. Phys.* **1949**, *17*, 602−606.
(2) Gordon, G.; Taube, H. *J. Inorg. Nucl. Chem.* **1961**, *16*, 272−278.
(3) Clark, D. L.; Conradson, S. D.; Donohoe, R. J.; Keogh, D. W.; Morris, D. E.; Palmer, P. D.; Rogers, R. D.; Tait, C. D. *Inorg. Chem.* **1999**, *38*, 1456−1466.
(4) Szabo, Z.; Grenthe, I. *Inorg. Chem.* **2007**, *46*, 9372−9378.
(5) Szabo, Z.; Grenthe, I. *Inorg. Chem.* **2010**, *49*, 4928−4933.
(6) Fortier, S.; Hayton, T. W. *Coord. Chem. Rev.* **2010**, *254*, 197−214.
(7) Wahlin, P.; Danilo, C.; Vallet, V.; Réal, F.; Flament, J. P.; Wahlgren, U. *J. Chem. Theory Comput.* **2008**, *4*, 569−577.
(8) Réal, F.; Vallet, V.; Wahlgren, U.; Grenthe, I. *J. Am. Chem. Soc.* **2008**, *130*, 11742−11751.
(9) Shamov, G. A.; Schreckenbach, G. *J. Am. Chem. Soc.* **2008**, *130*, 13735−13744.
(10) Schreckenbach, G.; Shamov, G. A. *Acc. Chem. Res.* **2010**, *43*, 19−29.
(11) Bühl, M.; Schreckenbach, G. *Inorg. Chem.* **2010**, *49*, 3821−3827.
(12) Bühl, M.; Wipff, G. *ChemPhysChem* **2011**, *12*, 3095−3105.
(13) Tsushima, S. *Inorg. Chem.* **2012**, *51*, 1434−1439.
(14) Rabideau, S. W.; Masters, B. J. *J. Phys. Chem.* **1963**, *67*, 318−323.
(15) Rabideau, S. W. *J. Phys. Chem.* **1963**, *67*, 2655−2659.
(16) Blum, O.; Stöckigt, D.; Schröder, D.; Schwarz, H. *Angew. Chem., Int. Ed.* **1992**, *31*, 603−604.
(17) Brönstrup, M.; Schröder, D.; Schwarz, H. *Chem.—Eur. J.* **1999**, *5*, 1176−1185.
(18) Bärsch, S.; Schröder, D.; Schwarz, H. *Chem.—Eur. J.* **2000**, *6*, 1789−1796.
(19) Jackson, P.; Harvey, J. N.; Schröder, D.; Schwarz, H. *Int. J. Mass Spectrom.* **2001**, *204*, 233−245.
(20) Koyanagi, G. K.; Bohme, D. K.; Kretzschmar, I.; Schröder, D.; Schwarz, H. *J. Phys. Chem. A* **2001**, *105*, 4259−4271.
(21) Gronert, S. *J. Am. Soc. Mass Spectrom.* **1998**, *9*, 845−848.
(22) Rios, D.; Rutkowski, P. X.; Shuh, D. K.; Bray, T. H.; Gibson, J. K.; Van Stipdonk, M. J. *J. Mass Spectrom.* **2011**, *46*, 1247−1254.
(23) Rutkowski, P. X.; Michelini, M. C.; Bray, T. H.; Russo, N.; Marçalo, J.; Gibson, J. K. *Theor. Chem. Acc.* **2011**, *129*, 575−592.
(24) Becke, A. D. *J. Chem. Phys.* **1993**, *98*, 5648−5652.
(25) Lee, C. T.; Yang, W. T.; Parr, R. G. *Phys. Rev. B* **1988**, *37*, 785−789.
(26) Küchle, W.; Dolg, M.; Stoll, H.; Preuss, H. *J. Chem. Phys.* **1994**, *100*, 7535−7542.
(27) Krishnan, R.; Binkley, J. S.; Seeger, R.; Pople, J. A. *J. Chem. Phys.* **1980**, *72*, 650−654.
(28) Blaudeau, J. P.; McGrath, M. P.; Curtiss, L. A.; Radom, L. *J. Chem. Phys.* **1997**, *107*, 5016−5021.
(29) Clark, T.; Chandrasekhar, J.; Spitznagel, G. W.; Schleyer, P. V. *J. Comput. Chem.* **1983**, *4*, 294−301.
(30) Gonzalez, C.; Schlegel, H. B. *J. Chem. Phys.* **1989**, *90*, 2154−2161.
(31) Gonzalez, C.; Schlegel, H. B. *J. Phys. Chem.* **1990**, *94*, 5523−5527.
(32) Fonseca Guerra, C.; Snijders, J. G.; te Velde, G.; Baerends, E. J. *Theor. Chem. Acc.* **1998**, *99*, 391−403.
(33) Te Velde, G.; Bickelhaupt, F. M.; Van Gisbergen, S. J. A.; Fonseca Guerra, C.; Baerends, E. J.; Snijders, J. G.; Ziegler, T. *J. Comput. Chem.* **2001**, *22*, 931−967.
(34) Frisch, M. J.; et al. Gaussian 2009 (revision B.01). See Supporting Information for full citation.
(35) Michelini, M. C.; Russo, N.; Sicilia, E. *Angew. Chem., Int. Ed.* **2006**, *45*, 1095−1099.

(36) Michelini, M. C.; Russo, N.; Sicilia, E. *J. Am. Chem. Soc.* **2007**, *129*, 4229−4239.
(37) Rios, D.; Michelini, M. C.; Lucena, A. F.; Marçalo, J.; Gibson, J. K. *Inorg. Chem.* **2012**, *51*, 6603−6614.
(38) Shamov, G. A.; Schreckenbach, G. *J. Phys. Chem. A* **2005**, *109*, 10961−10974.
(39) Cao, A.; Balasubramanian, K. *J. Chem. Phys.* **2009**, *131*, 164504.
(40) Glendening, E. D.; Reed, A. E.; Carpenter, J. E.; Weinhold, F.; *NBO 3.1* ed.
(41) Bader, R. F. W. *Atoms in Molecules: A Quantum Theory*; Oxford University Press: Oxford, U.K., 1994.
(42) Becke, A. D.; Edgecombe, K. E. *J. Chem. Phys.* **1990**, *92*, 5397−5403.
(43) Silvi, B.; Savin, A. *Nature* **1994**, 683−686.
(44) Noury, S.; Krokidis, X.; Fuster, F.; Silvi, B.; TopMod package ed.; Universitè Pierre et Marie Curie: Paris, France, 1997.
(45) Su, T.; Chesnavich, W. J. *J. Chem. Phys.* **1982**, *76*, 5183−5185.
(46) Marçalo, J.; Gibson, J. K. *J. Phys. Chem. A* **2009**, *113*, 12599−12606.
(47) Gibson, J. K.; Haire, R. G.; Santos, M.; Marçalo, J.; de Matos, A. P. *J. Phys. Chem. A* **2005**, *109*, 2768−2781.
(48) Barros, N.; Maynau, D.; Maron, L.; Eisenstein, O.; Zi, G. F.; Andersen, R. A. *Organometallics* **2007**, *26*, 5059−5065.
(49) Eisenstein, J. C. *J. Chem. Phys.* **1956**, *25*, 142−146.
(50) Denning, R. G.; Snellgrove, T. R.; Woodwark, D. R. *Mol. Phys.* **1979**, *37*, 1109−1143.
(51) Tatsumi, K.; Hoffmann, R. *Inorg. Chem.* **1980**, *19*, 2656−2658.
(52) Denning, R. G. *Struct. Bonding (Berlin)* **1992**, *79*, 215−276.
(53) Denning, R. G.; Green, J. C.; Hutchings, T. E.; Dallera, C.; Tagliaferri, A.; Giarda, K.; Brookes, N. B.; Braicovich, L. *J. Chem. Phys.* **2002**, *117*, 8008−8020.
(54) Denning, R. G. *J. Phys. Chem. A* **2007**, *111*, 4125−4143.
(55) Glueckauf, E.; Mckay, H. A. C. *Nature* **1950**, *165*, 594−595.
(56) Kaltsoyannis, N.; Bursten, B. E. *Inorg. Chem.* **1995**, *34*, 2735−2744.
(57) Ingram, K. I. M.; Tassell, M. J.; Gaunt, A. J.; Kaltsoyannis, N. *Inorg. Chem.* **2008**, *47*, 7824−7833.
(58) Tassell, M. J.; Kaltsoyannis, N. *Dalton Trans.* **2010**, *39*, 6719−6725.
(59) Kirker, I.; Kaltsoyannis, N. *Dalton Trans.* **2011**, *40*, 124−131.
(60) Prodan, I. D.; Scuseria, G. E.; Martin, R. L. *Phys. Rev. B* **2007**, *76*, 033101/1−033106/4.
(61) Minasian, S. G.; Keith, J. M.; Batista, E. R.; Boland, K. S.; Clark, D. L.; Conradson, S. D.; Kozimor, S. A.; Martin, R. L.; Schwarz, D. E.; Shuh, D. K.; Wagner, G. L.; Wilkerson, M. P.; Wolfsberg, L. E.; Yang, P. *J. Am. Chem. Soc.* **2012**, *134*, 5586−5597.
(62) Kaltsoyannis, N. *Inorg. Chem.* **2012**, DOI: 10.1021/ic3006025.
(63) Gresham, G. L.; Gianotto, A. K.; Harrington, P. D.; Cao, L. B.; Scott, J. R.; Olson, J. E.; Appelhans, A. D.; Van Stipdonk, M. J.; Groenewold, G. S. *J. Phys. Chem. A* **2003**, *107*, 8530−8538.
(64) Groenewold, G. S.; Cossel, K. C.; Gresham, G. L.; Gianotto, A. K.; Appelhans, A. D.; Olson, J. E.; Van Stipdonk, M. J.; Chien, W. *J. Am. Chem. Soc.* **2006**, *128*, 3075−3084.
(65) Bryantsev, V. S.; de Jong, W. A.; Cossel, K. C.; Diallo, M. S.; Goddard, W. A.; Groenewold, G. S.; Chien, W.; Van Stipdonk, M. J. *J. Phys. Chem. A* **2008**, *112*, 5777−5780.